HIGH DYNAMIC RANGE LIGHT FIELDS VIA WEIGHTED LOW RANK APPROXIMATION

Mikaël Le Pendu ⋆, *Christine Guillemot* †, *Aljosa Smolic* ⋆

⋆ Trinity College Dublin (TCD), Dublin 2, Ireland
† INRIA, Campus de Beaulieu, 35042 Rennes Cedex, France

ABSTRACT

In this paper, we propose a method for capturing High Dynamic Range (HDR) light fields with dense viewpoint sampling. Analogously to the traditional HDR acquisition process, several light fields are captured at varying exposures with a plenoptic camera. The RAW data is de-multiplexed to retrieve all light field viewpoints for each exposure and perform a soft detection of saturated pixels. Considering a matrix which concatenates all the vectorized views, we formulate the problem of recovering saturated areas as a Weighted Low Rank Approximation (WLRA) where the weights are defined from the soft saturation detection. We show that our algorithm successfully recovers the parallax in the over-exposed areas while the Truncated Nuclear Norm (TNN) minimization, traditionally used for single view HDR imaging, does not generalize to light fields. Advantages of our weighted approach as well as the simultaneous processing of all the viewpoints are also demonstrated in our experiments.

Index Terms— High Dynamic Range (HDR), Light Fields, Low Rank Matrix Completion, Weighted Low Rank Approximation.

1. INTRODUCTION

The emerging technologies in light field capture and HDR imaging allow increased freedom for content creation and manipulation by producing a richer description of a scene than traditional images. For instance, light fields make it possible to change the focus after taking a picture and HDR images can be freely re-exposed without unveiling either noise in dark areas or saturated pixels in the bright parts of the image. A light field is typically represented as an array of viewpoints. Many capture systems have been designed, including camera arrays, single cameras mounted on moving gantries and plenoptic cameras with a micro-lens array placed in front of the sensor. Regarding HDR images, their acquisition generally involves taking several pictures of the scene at different exposures. A large panel of methods have been developed for merging the captured images into an HDR one, including patch-based methods [1–3], Low Rank Matrix Completion (LRMC) [4–7], and more recently deep learning [8]. A comprehensive review of the subject is provided in [9].

While both HDR and light field imaging have received a lot of attention, only a few attempts have been made at combining these technologies. Manakov et al. [10] have developed a camera add-on capable of transforming a standard camera into either a HDR or a light field camera. In [11, 12], a focused plenoptic camera with a micro-lens aperture pattern is designed to capture an HDR image in a single shot. However, the authors of [10–12] do not discuss the simultaneous HDR and light field capture.

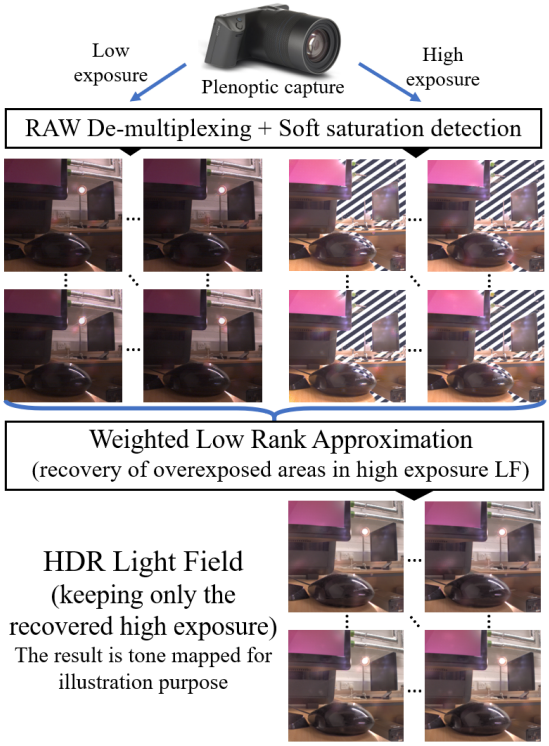

Fig. 1. HDR Light Field acquisition pipeline.

Based on a camera array setup, the method in [13] is able to capture HDR light field videos by varying the exposure time both sequentially (between successive frames) and spatially (over the different cameras). Note that the sparse view sampling resulting from the large baseline of camera array devices causes strong angular aliasing when generating refocused images from the light field (i.e. sharp structures in the out of focus areas). This issue is observed in the results of [13]. Similarly, related methods in multiview HDR capture [14] are not suitable for light field rendering that require dense viewpoint sampling. Finally, Li et al. [15] capture multiple exposures with a plenoptic camera and merge them into a HDR light field by applying directly the method of Debevec and Malik [16] to 4D light fields instead of 2D images. This can be seen as treating each viewpoint independently. However, the method in [16] is known for requiring many different exposures with overlapping well-exposed areas, which complicates the acquisition task. Furthermore, the large amount of data to process increases the computational load, particularly for light fields with densely sampled viewpoints.

In this paper, we propose a new HDR light field acquisition method based on multiple plenoptic captures (typically two or

three) with varying exposure as depicted in Fig.1. By taking the highest exposure as a reference, generating the HDR light field amounts to recovering the saturated areas using the lower exposure captures. For that purpose, soft detection of the saturated pixels is performed from the RAW data. It accounts for the fact that in practice, sensor response is not linear close to saturation. The whole set of views (all sub-aperture images at all exposures) is then arranged in a matrix where each column is a vectorized view. The matrix is completed with Weighted Low Rank Approximation (WLRA) naturally exploiting the redundancies between views. General background on WLRA can be found in [17]. In our approach, the problem is solved by extending the matrix completion algorithm of [18] to non-binary weights, thus accounting for the soft saturation model. We show that our non-binary approach better handles the transition between the saturated and non-saturated areas. Furthermore, unlike the the Truncated Nuclear Norm minimization previously used in several HDR imaging methods [4–7], our rank minimization successfully applies to light fields where the rank is expected to be higher than 1 because of the parallax. We additionally discuss the advantages of processing all the viewpoints simultaneously.

2. RAW DATA PROCESSING

2.1. De-multiplexing and Soft Saturation Detection

The plenoptic RAW data is first de-multiplexed into light field views by adapting the method in [19] (we use the enhancements in [20]). In order to exploit the full dynamic range of each captured light field, we removed the clipping operations previously used for pixels close to saturation. Instead, soft saturation detection is performed directly on sensor data (i.e. before the devignetting and demosaicing steps of [19]). For a pixel of normalized value x, we compute its saturation $s(x) = \min((x + (1 - \tau))^{12}, 1)$ as illustrated in Fig.2. In practice, even if a pixel is not fully saturated ($x < 1$), neighboring pixels associated to the other color components on the bayer pattern may saturate. Hence, the level of full saturation τ is set to 0.9 to account for unreliable colors of high pixel values.

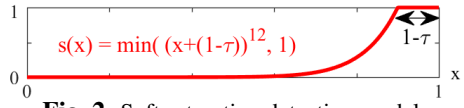

Fig. 2. Soft saturation detection model.

Similarly to the color data, the sensor saturation image is demultiplexed using [19] (without devignetting and demosaicing) to obtain a saturation map of each light field view.

2.2. Construction of Matrices for WLRA

In order to cope with possible movements of the camera when capturing the different exposures, a homography alignment is performed. For fast computations, homography parameters are determined only from the central views of the high and low exposure light fields employing homography based low rank approximation (HLRA) [21]. All the views of the low exposure light fields are then aligned to the high exposure one using the same homography. Prior to the WLRA, we convert RGB data to luminance Y and CIE chromaticity components $u'v'$. Independent processing of the Y, u' and v' components has been shown in [18] to be advantageous both in terms of quality and computing speed for light field completion with low rank matrix approximation. Additional conversion of the saturation s into weights w is also necessary to perform weighted low rank approximation:

$$w = \frac{1 - s}{s + 1/w_{max}}. \tag{1}$$

The non-saturated pixels ($s = 0$) are thus associated to the maximum weight w_{max} indicating a high confidence, while the fully saturated pixels ($s = 1$) have a null weight. In our experiments, we use $w_{max} = 100$.

Finally, weights and image data are arranged into respective matrices W and $M \in \mathbb{R}^{m \times n}$ such that each column contains a vectorized light field view (n is the total number of views including all exposures and m is the number of pixels per view). In the case where an object is over-exposed even in the lowest exposure, some rows of the matrix may have only unknown elements (zero weight). This may result in arbitrary completed values in these areas. In order to avoid this situation, the weights of all the views of the lowest exposure are set to w_{max}.

3. WEIGHTED LOW RANK APPROXIMATION

3.1. General Formulation

Our WLRA method generalizes the matrix completion algorithm in [18] to the case of non-binary weights. While most methods, relying on the results of [22], solve a simpler convex problem by minimizing the nuclear norm (i.e. sum of singular values), the algorithm in [18] keeps the rank in the objective function and solves the problem using the Alternating Direction Method of Multipliers (ADMM) [23]. We use the same approach as it was shown to outperform conventional matrix completion for the closely related light field inpainting application. Given the matrix M to approximate, a global noise tolerance parameter ϵ, and the element-wise weight matrix W, the problem formulation is:

$$\begin{aligned} \min_{X} \quad & \operatorname{rank}(X) \\ \text{s.t.} \quad & X = Z \\ & \|W \circ (Z - M)\|_F^2 \leq \epsilon, \end{aligned} \tag{2}$$

where the operator $\circ$ is the element-wise multiplication. The introduction of the matrix Z and the constraint $X = Z$ makes it possible to use the Alternating Direction Method of Multipliers. The constraint $X = Z$ is taken into account by defining the augmented Lagrangian function:

$$\mathcal{L}(X, Z, \Lambda, \rho) = \operatorname{rank}(X) + \operatorname{Tr}(\Lambda^\top (X - Z)) + \frac{\rho}{2} \|X - Z\|_F^2, \tag{3}$$

where Λ is a matrix of lagrangian multipliers and ρ is a positive scalar. At each iteration k, the ADMM algorithm for our WLRA problem then consists in updating X, Z, Λ, and ρ as:

$$X_k = \arg\min_{X} \mathcal{L}(X, Z_{k-1}, \Lambda_{k-1}, \rho_{k-1}), \tag{4}$$

$$Z_k = \arg\min_{Z \text{ s.t. } \|W \circ (Z-M)\|_F^2 \leq \epsilon} \mathcal{L}(X_k, Z, \Lambda_{k-1}, \rho_{k-1}), \tag{5}$$

$$\Lambda_k = \Lambda_{k-1} + \rho_{k-1} \cdot (X_k - Z_k), \tag{6}$$

$$\rho_k = t \cdot \rho_{k-1} \qquad (\text{with } t > 1), \tag{7}$$

where t is a parameter controlling the tradeoff between accurate minimization ($t \approx 1$) and fast convergence ($t \gg 1$). For our HDR light field application, we use $t = 1.1$ and $t = 4$ respectively for the luminance and the chromaticity components.

In the following subsections we describe how to efficiently solve the X and Z sub-problems introduced in Eqs. (4) and (5) respectively. For simplicity of notation, the iteration indices k are ignored in the rest of the paper.

3.2. X sub-problem

Defining $\mathbb{H}_\tau$ as the singular value hard thresholding operator with threshold τ, it was shown in [18] that the X sub-problem in Eq.(4) has a closed form solution given by:

$$\arg\min_X \mathcal{L}(X, Z, \Lambda, \rho) = \mathbb{H}_{\sqrt{\frac{2}{\rho}}}\left(Z - \frac{\Lambda}{\rho}\right). \tag{8}$$

3.3. Z sub-problem

The Z sub-problem in Eq.(5), can be equivalently rewritten:

$$\begin{aligned} &\arg\min_Z \|N - Z\|_F^2 \\ &\text{s.t. } \|W \circ (Z - M)\|_F^2 \leq \epsilon, \end{aligned} \tag{9}$$

where $N = X + \frac{\Lambda}{\rho}$. Let us define the Lagrangian function:

$$\mathcal{L}_Z(Z, \lambda) = \|N - Z\|_F^2 + \lambda\left(\|W \circ (M - Z)\|_F^2 - \epsilon\right). \tag{10}$$

By deriving the stationary condition (i.e. $\frac{\partial \mathcal{L}_Z}{\partial \mathbf{Z}}(\mathbf{Z}) = 0$), we obtain the following expression of Z for all entries Z_{ij}:

$$Z_{ij} = (N_{ij} + \lambda W_{ij}^2 \cdot M_{ij})/(1 + \lambda W_{ij}^2). \tag{11}$$

In order to determine the value of the lagrangian multiplier λ such that Z is the solution of Eq.(9), we use the Karush-Kuhn-Tucker complementary slackness conditions:

$$\lambda \geq 0 \tag{12}$$

$$\lambda = 0 \quad \text{or} \quad f \triangleq \|W \circ (M - Z)\|_F^2 - \epsilon = 0. \tag{13}$$

The expression f in Eq.(13) can be seen as a function of λ by replacing Z by its expression of Eq.(11). We obtain:

$$f(\lambda) = \sum_{i,j}\left(\frac{W_{ij}(M_{ij} - N_{ij})}{1 + \lambda W_{ij}^2}\right)^2 - \epsilon = 0. \tag{14}$$

As Eq.(14) does not have a closed form solution for λ, we solve it numerically. The value of λ is initialized as 0 and is iteratively updated following Newton's method, by subtracting $\frac{f(\lambda)}{f'(\lambda)}$, where the derivative f' of f is given by:

$$f'(\lambda) = \sum_{i,j}\frac{-2W_{ij}^2}{1 + \lambda W_{ij}^2} \cdot \left(\frac{W_{ij}(M_{ij} - N_{ij})}{1 + \lambda W_{ij}^2}\right)^2. \tag{15}$$

Note that f is monotonically decreasing on $\mathbb{R}^+$. Thus, if $f(0) < 0$, there is no positive solution to Eq.(14). In this case, the value of λ satisfying the conditions (12), (13) as well as the constraint in Eq.(9) is 0, and no further iteration is required. Otherwise, there is a unique positive solution. In practice, for our problem, less than 10 iterations are usually required to find λ with the stopping criterion: $|f(\lambda)| < 10^{-4}$.

In order to accelerate each iteration of the λ computation, the elements of the input weight matrix W are quantized to a limited set of values $\{w_q\}_{q \in [\![1, q_{max}]\!]}$. Then, instead of computing f and f' by summing terms over all matrix elements i, j, they are determined as a sum of only q_{max} terms:

$$f(\lambda) = \sum_{q=1}^{q_{max}}\left(\frac{w_q^2}{(1 + \lambda w_q^2)^2} \cdot R_q\right) - \epsilon, \tag{16}$$

$$f'(\lambda) = \sum_{q=1}^{q_{max}}\left(\frac{-2w_q^2}{1 + \lambda w_q^2} \cdot \frac{w_q^2}{(1 + \lambda w_q^2)^2} \cdot R_q\right), \tag{17}$$

where R_q is the sum of squared residuals between M and N only accounting for the elements associated to the weight w_q. As R_q does not depend on λ, it only needs to be computed once as:

$$R_q = \sum_{i,j}(M_{ij} - N_{ij})^2 \cdot \delta_{w_q}^{W_{ij}}, \tag{18}$$

with δ the Kronecker delta (equal to 1 if $w_q = W_{ij}$ and 0 otherwise). Using this method with a number of weight values $q_{max} = 256$, the computing cost of λ is negligible with respect to the rest of the algorithm. Hence, the per-iteration cost of our WLRA method is not increased compared to the algorithm [18] restricted to binary weights. Additional discussion on computing cost is given in the next section.

4. EXPERIMENTAL RESULTS

For all our experiments, light fields are captured using a Lytro Illum camera. We first validate the choice of the rank minimization formulation by comparing our results with those obtained by replacing the rank in Eq.(2) by the Truncated Nuclear Norm $\|X\|_r$ (sum of the singular values excluding the r highest ones). This problem is solved by replacing the hard thresholding in Eq.(8) by the Partial Singular Value Thresholding operator $\mathbb{P}_{r, \frac{1}{\rho}}$ defined in [24]. For both rank and TNN minimizations, Z is initialized as $Z_0 = M$. In order to use the same parameterization for all the experiments, we define the normalization factor $\nu = \|W \circ M\|_F^2$ and we use the parameter $\epsilon = 0.003 \cdot \nu$ for the luminance component, and $\epsilon = 0.04 \cdot \nu$ for the $u'v'$ components. For our rank minimization, the penalty parameter ρ is initialized according to [18] as $\rho_0 = 8/(\sigma_1 + \sigma_2)^2$ (with σ_1 and σ_2 the two largest singular

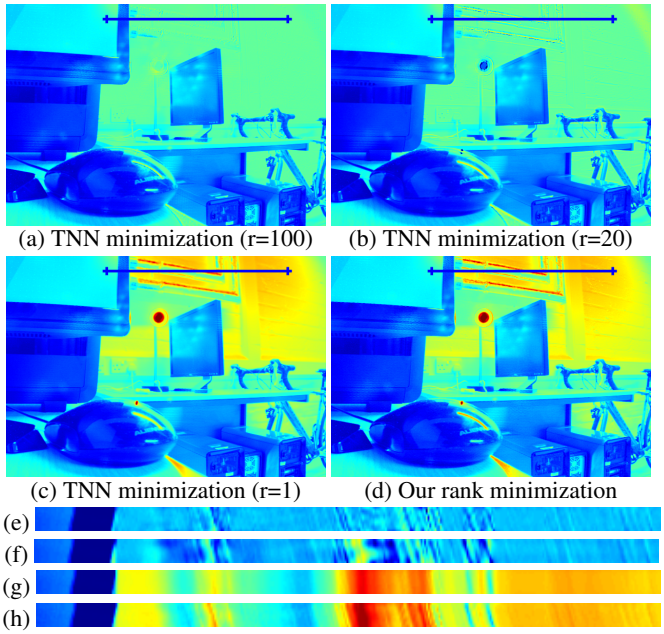

(a) TNN minimization (r=100) (b) TNN minimization (r=20)

(c) TNN minimization (r=1) (d) Our rank minimization

(e) (f) (g) (h)

Fig. 3. 13x13 HDR Light field reconstructed from 3 exposures: (a)-(d) show the central view in false color for each method. (e),(f),(g),(h) are the epipolar images corresponding to the blue segment in (a),(b),(c),(d) respectively (vertical axis shows vertical viewpoint change). The epipolar image in (g) shows that the structures completed using TNN minimization with r=1 are blurred and identical in all the views (parallax is not preserved).

(a) High Exposure (b) Low Exposure

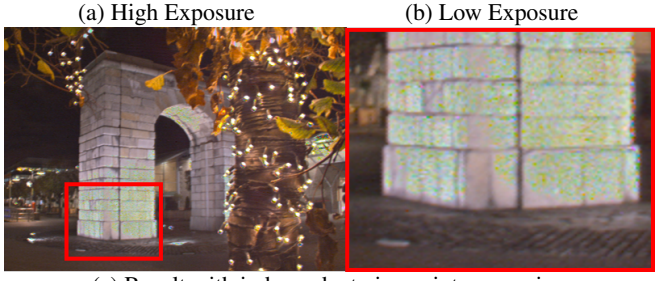

(c) Result with independent viewpoint processing

(d) Result with simultaneous viewpoint processing

Fig. 4. Comparison between independent and simultaneous processing of the viewpoints. Some over-exposed areas in the high exposure capture (a) are under-exposed in the low exposure one (b). Independent processing of the viewpoints (c) highlights the presence of noise due to under-exposition in (b). Using all the viewpoints in the WLRA (d) naturally exploits redundancies to reduce the noise. (c) and (d) are tone mapped for display purpose.

values of M). For TNN minimization, we use $\rho_0 = 1.25/\sigma_1$ as suggested in [7].

In single view HDR imaging, existing low rank based methods [4–7] minimize the TNN with $r = 1$ as the matrix rank can be assumed to be 1. However, this assumption does not hold for light fields with disparities between views, and produces blur in the completed regions as shown in Fig.3(c),(g). Using higher values of r keeps the details but not the low spatial frequencies (Fig.3(a),(b),(e),(f)). Our rank minimization successfully recovers both low and high frequencies (Fig.3(d),(h)).

Fig.4 provides further justification of our approach compared to independently applying the WLRA to each viewpoint. By considering all the viewpoints simultaneously, our method is able to reduce the noise, and thus addresses the challenging case of large exposure gaps where some saturated areas of the high exposure capture are under-exposed and noisy in the low exposure one. Note that with a simultaneous processing of all the views, our method may also apply for correcting artifacts that are not consistent between the views (e.g. lens flare) as long as the artifacts can be detected and taken into account in the weights.

We finally illustrate in Fig.5 the advantage of using a weighted low rank approximation along with soft saturation detection instead of the matrix completion of [18] that requires

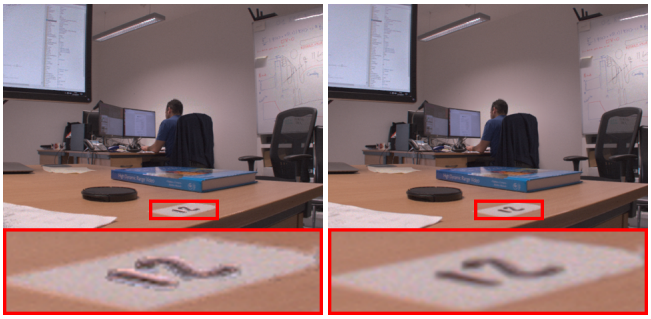

(a) Binary weigths (LRMC [18]) (b) Non-binary weigths (WLRA)

Fig. 5. Recovered saturated areas from two exposures using: (a) Low Rank Matrix Completion of [18] (binary weights), (b) our WLRA (non-binary weigths). In this example, the white parts of the label were saturated in the high exposure capture. Traditional matrix completion produces artifacts at the boundary of these regions.

binary weights. Note that in this example, the matrix size is 267030×98 (2 exposures for 7×7 views of size 430×621). With our Matlab implementation, the processing time was 54.4s for WLRA (respectively 103, 8 and 8 iterations for Y,u',v'), and 54.8s for the low rank matrix completion (respectively 104, 8 and 8 iterations for Y,u',v'). Hence, for our application, the proposed extension of matrix completion to non-binary weights does not affect the convergence speed and has similar computing cost.

5. CONCLUSION

We have presented a new method for the acquisition of high dynamic range, densely sampled light fields, using successive plenoptic captures at varying exposures. In order to recover the saturated regions of the high exposure light field, we have defined a new weighted low rank approximation algorithm. It exploits simultaneously the information of all the viewpoints at all exposures, as well as soft saturation maps previously extracted from the RAW data. We have shown that, unlike the low rank methods used in single view HDR acquisition, our algorithm remains suitable for processing dense light fields with parallax. Our weighted approach also produces more natural results than traditional low rank matrix completion. One can note that we do not address the case of dynamic scenes if moving objects are partly saturated in the high exposure capture. However, we have shown that the proposed algorithm remains effective with large gaps between exposures, thus simplifying the acquisition task.

As a final note, the simultaneous processing of all the views allows for potential extension to plenoptic devices generating differently exposed or filtered viewpoints in a single capture. Although existing lenslet-based plenoptic cameras already present such characteristics (darker external views caused by vignetting of the micro-lenses), this is not sufficient to significantly increase the dynamic range. Hence, further research is necessary to achieve instantaneous capture of HDR light fields.

6. ACKNOWLEDGEMENT

This project has been supported in part by the Science Foundation Ireland (SFI) under the Grant Number 15/RP/2776 and in part by the EU H2020 Research and Innovation Programme under grant agreement No 694122 (ERC advanced grant CLIM).

7. REFERENCES

[1] J. Hu, O. Gallo, K. Pulli, and X. Sun, "Hdr deghosting: How to deal with saturation ?," in *CVPR*, 2013.

[2] P. Sen, N. K. Kalantari, M. Yaesoubi, S. Darabi, D. B. Goldman, and E. Shechtman, "Robust Patch-Based HDR Reconstruction of Dynamic Scenes," *ACM Transactions on Graphics (TOG) (Proceedings of SIGGRAPH Asia 2012)*, vol. 31, no. 6, pp. 203:1–203:11, 2012.

[3] O. Gallo, A. Troccoli, J. Hu, K. Pulli, and J. Kautz, "Locally non-rigid registration for mobile hdr photography," in *IEEE Conference on Computer Vision and Pattern Recognition Workshops (CVPRW)*, Jun. 2015, vol. 00, pp. 48–55.

[4] T. H. Oh, J. Y. Lee, Y. W. Tai, and I. S. Kweon, "Robust high dynamic range imaging by rank minimization," *IEEE Transactions on Pattern Analysis and Machine Intelligence*, vol. 37, no. 6, pp. 1219–1232, Jun. 2015.

[5] C. Lee, Y. Li, and V. Monga, "Ghost-free high dynamic range imaging via rank minimization," *IEEE Signal Processing Letters*, vol. 21, no. 9, pp. 1045–1049, Sep. 2014.

[6] C. Lee and E. Y. Lam, "High dynamic range imaging via truncated nuclear norm minimization of low-rank matrix," in *2016 IEEE International Conference on Acoustics, Speech and Signal Processing (ICASSP)*, Mar. 2016, pp. 1229–1233.

[7] C. Lee and E. Y. Lam, "Computationally efficient truncated nuclear norm minimization for high dynamic range imaging," *IEEE Transactions on Image Processing*, vol. 25, no. 9, pp. 4145–4157, Sep. 2016.

[8] N. K. Kalantari and R. Ramamoorthi, "Deep high dynamic range imaging of dynamic scenes," *ACM Trans. Graph.*, vol. 36, no. 4, pp. 144:1–144:12, Jul. 2017.

[9] O. Gallo and P. Sen, "Chapter 3 - stack-based algorithms for HDR capture and reconstruction," in *High Dynamic Range Video*, Frédéric Dufaux, Patrick Le Callet, Rafal K. Mantiuk, and Marta Mrak, Eds., pp. 85 – 119. Academic Press, 2016.

[10] A. Manakov, J. F. Restrepo, O. Klehm, R. Hegedüs, E. Eisemann, H.-P. Seidel, and I. Ihrke, "A reconfigurable camera add-on for high dynamic range, multispectral, polarization, and light-field imaging," *ACM Trans. Graph.*, vol. 32, no. 4, pp. 47:1–47:14, Jul. 2013.

[11] T. G. Georgiev, A. Lumsdaine, and S. Goma, "High dynamic range image capture with plenoptic 2.0 camera," in *Frontiers in Optics 2009/Laser Science XXV/Fall 2009 OSA Optics & Photonics Technical Digest*. 2009, p. SWA7P, Optical Society of America.

[12] T. G. Georgiev, A. Lumsdaine, and G. Chunev, "Using focused plenoptic cameras for rich image capture," *IEEE Computer Graphics and Applications*, vol. 31, no. 1, pp. 62–73, Jan. 2011.

[13] D. C. Schedl, C. Birklbauer, and O. Bimber, "Coded exposure hdr light-field video recording," *Computer Graphics Forum*, 2014.

[14] R.R. Orozco, C. Loscos, I. Martin, and A. Artusi, "Chapter 3 - HDR multiview image sequence generation: Toward 3d HDR video," in *High Dynamic Range Video*, Alan Chalmers, Patrizio Campisi, Peter Shirley, and Igor G. Olaizola, Eds., pp. 61 – 86. Academic Press, 2017.

[15] C. Li and X. Zhang, "High dynamic range and all-focus image from light field," in *2015 IEEE 7th International Conference on Cybernetics and Intelligent Systems (CIS) and IEEE Conference on Robotics, Automation and Mechatronics (RAM)*, Jul. 2015, pp. 7–12.

[16] P. E. Debevec and J. Malik, "Recovering high dynamic range radiance maps from photographs," in *ACM SIGGRAPH 2008 Classes*, New York, NY, USA, 2008, SIGGRAPH '08, pp. 31:1–31:10, ACM.

[17] N. Srebro and T. Jaakkola, "Weighted low-rank approximations," in *Proceedings of the Twentieth International Conference on International Conference on Machine Learning*, 2003, ICML'03, pp. 720–727.

[18] M. Le Pendu, X. Jiang, and C. Guillemot, "Light field inpainting propagation via low rank matrix completion," *IEEE Transactions on Image Processing*, vol. 27, no. 4, pp. 1981–1993, Apr. 2018.

[19] D. G. Dansereau, O. Pizarro, and S. B. Williams, "Decoding, calibration and rectification for lenselet-based plenoptic cameras," in *Proc. CVPR*, 2013, pp. 1027–1034.

[20] P. David, M. Le Pendu, and C. Guillemot, "White lenslet image guided demosaicing for plenoptic cameras," in *IEEE 19th International Workshop on Multimedia Signal Processing (MMSP)*, Oct. 2017, pp. 1–6.

[21] X. Jiang, M. Le Pendu, R. A. Farrugia, and C. Guillemot, "Light field compression with homography-based low-rank approximation," *IEEE Journal of Selected Topics in Signal Processing*, vol. 11, no. 7, pp. 1132–1145, Oct. 2017.

[22] E. Candès and B. Recht, "Exact matrix completion via convex optimization," *Commun. ACM*, vol. 55, no. 6, pp. 111–119, Jun. 2012.

[23] S. Boyd, N. Parikh, E. Chu, B. Peleato, and J. Eckstein, "Distributed optimization and statistical learning via the alternating direction method of multipliers," *Found. Trends Mach. Learn.*, vol. 3, no. 1, pp. 1–122, Jan. 2011.

[24] T. H. Oh, H. Kim, Y. W. Tai, J. C. Bazin, and I. S. Kweon, "Partial sum minimization of singular values in rpca for low-level vision," in *2013 IEEE International Conference on Computer Vision*, Dec. 2013, pp. 145–152.